Published in final edited form as:
Phys Chem Chem Phys. 2012 May 14; 14(18): 6192–6199. doi:10.1039/c2cp23587k.

Ultrafast spin-state photoswitching in a crystal and slower consecutive processes investigated by femtosecond optical spectroscopy and picosecond X-ray diffraction

Eric Collet[a], **Nicolas Moisan**[a], **Chérif Baldé**[a], **Roman Bertoni**[a], **Elzbieta Trzop**[b], **Claire Laulhé**[c], **Maciej Lorenc**[a], **Marina Servol**[a], **Hervé Cailleau**[a], **Antoine Tissot**[d], **Marie-Laure Boillot**[d], **Timothy Graber**[e], **Robert Henning**[e], **Philip Coppens**[c], and **Marylise Buron-Le Cointe**[a]

Eric Collet: eric.collet@univ-rennes1.fr

[a]Institut de Physique de Rennes, UMR 6251 UR1-CNRS, Bat 11A Campus de Beaulieu, University Rennes 1, Rennes, France. Fax: 33 223236717; Tel: 33 223236532

[b]Chemistry Department, University at Buffalo, State University of New York, Buffalo, NY 14260-3000, USA

[c]Synchrotron SOLEIL, L'Orme des Merisiers, Saint Aubin B.P. 48, 91192 Gif-sur-Yvette, France

[d]Institut de Chimie Moléculaire et Matériaux d'Orsay, UMR-CNRS 8182, Université Paris-Sud 11, Orsay, France

[e]The Consortium for Advanced Radiation Sources, University of Chicago, Chicago, IL 60637, USA

Abstract

We report the spin state photo-switching dynamics in two polymorphs of a spin-crossover molecular complex triggered by a femtosecond laser flash, as determined by combining femtosecond optical pump-probe spectroscopy and picosecond X-ray diffraction techniques,. The light-driven transformations in the two polymorphs are compared. Combining both techniques and tracking how the X-ray data correlate with optical signals allows understanding of how electronic and structural degrees of freedom couple and play their role when the switchable molecules interact in the active crystalline medium. The study sheds light on crossing the border between femtochemistry at the molecular scale and femtoswitching at the material scale

1 Introduction

With the advent of control science the current challenge is not only to observe matter on ever smaller scale but also to direct its functionality at the relevant length, time and energy scales. It is the aim of light-driven transformations, either under continuous light flux or a brief light pulse, to force the matter towards a new state far from thermal equilibrium for generating a photoinduced phase transition[1]. This opportunity to direct material properties by light promises impacting future technologies. Thus, spectacular switching of the macroscopic physical properties of materials resulting from an ultrafast light excitation were reported in different systems for switching from insulator to conductor[2–4], from paraelectric to ferroelectric[5,6], or between magnetic states[7–11]. Nevertheless, the understanding of

Correspondence to: Eric Collet, eric.collet@univ-rennes1.fr.

physical mechanisms involved in the transformation induced by an ultra-short femtosecond laser pulse is only emerging. Understanding and tracking how materials work, during elementary dynamical processes, has to face with several new and challenging basic questions. For instance, ultrafast information processing based on the control of light-driven switching of the physical properties of materials requires mastering how directing the system through a complex pathway from atomic to material scales and what fundamentally limits the transformation speed. This feat can be accomplished thanks to the increase of sophisticated instrumentation in ultrafast science. In addition to femtosecond optical pump-probe studies in solids or in solution, recent advances in time-resolved X-ray diffraction[12] make it now possible to probe structural processes at a much finer level than the time average studies allowed before.

More recently, the field of ultrafast photoinduced phase transitions has emerged within material science. If we attempt simple parallels here, the goal is then to realize at the level of a material what has been achieved at the level of a molecule in femtochemistry[13]. The photo-induced transformation pathway in a material is complex[14], as it is underlined here in spin-crossover materials, for which a magnetic molecular state may be photo-activated in a transient state. In the active medium, which the crystal is, other effects of elastic or thermal nature should be considered for describing the macroscopic response, as different processes spanning from molecular to material scales are linked together.

2 Spin-state photoswitching in a crystal

Crystals made of bistable magnetic molecules may be switched from Low Spin (LS) to High Spin (HS) states under the influence of various external perturbations, including laser excitation[7–11,15–20]. In these systems, the electronic distribution around the metal ion, with $3d^4$–$3d^7$ electronic configurations, of the constituting molecules can change from LS to HS when the octahedral environment of the ion is suitable, that is when the energies of LS and HS states are closely spaced. Then molecules can be easily inter-converted under external perturbations (temperature, pressure or light irradiation). In the spin-crossover process, the electron transfer is coupled to a sizeable structural reorganization of the inner and outer-sphere of coordination, accompanied by large changes of crystal volume[21–26].

Here we compare the photoresponse of two crystalline polymorphs of the molecular complex [(TPA)Fe(III)(TCC)]PF_6 [TPA = tris(2-pyridylmethyl)amine and TCC = 3,4,5,6-tetra-chlorocatecholate dianion]. One crystalline polymorph is monoclinic and the other orthorhombic and their structures, consisting of similar cation layers alternating with PF_6^- anion layers, mainly differ by the layer packing[27] along the crystal axis **b**. In addition to X-ray diffraction, optical identification of the two polymorphs is easy, since at room temperature the crystal colour is purple for the orthorhombic polymorph and orange for the monoclinic one, as illustrated in Fig. 1. The UV-vis-NIR spectra of the monoclinic and orthorhombic polymorphs recorded in the LS and HS phases are presented in Fig. S1 and indicate the iron(III) charge transfer absorption band (LMCT) of LS species centered at 890 nm.

To characterize the thermal spin conversion of both compounds, optical transmission measurements were performed at 480 and 600 nm with light polarized parallel to the long crystal axis (the crystallographic axis **a** for both polymorphs), which yields maximum transmission. By lowering the temperature both undergo a thermal spin-crossover between a high spin (S = 5/2) and a low spin (S = 1/2) state[27] with the thermal crossover only slightly shifted between the polymorphs: the characteristic temperatures $T_{1/2}$ corresponding to 50% conversion of the metal ions are 214 K for the monoclinic system and 203 K for the orthorhombic one. As observed in Fig. 1, the temperature dependence of the optical

properties when the HS molecular fraction changes from 0 to 1 as temperature increases are different for the polymorphs. In agreement with the change of colour, theoptical transmission (T) decreases for both at 480 nm, whereas at 600 nm it decreases for the orthorhombic form and increases for the monoclinic form. These optical changes provide are commonly used for monitoring the evolution of HS population at thermal equilibrium or under weak *cw* laser excitation[9,15,20,28]. Here we use it for probing ultrafast photoswitching dynamics in the solid state.

The intramolecular reorganization associated with the change of spin state occurs mainly around the central Fe ion (Fig. 2), and is characterized by the evolution of the bonds between the ion and the ligand[27]. For both polymorphs, the average <Fe-N> bond length changes from 1.96 Å (LS) to 2.13 Å (HS). As the fraction of molecules gradually changes from completely LS to HS, the above mentioned intramolecular structural change induces a gradual evolution of the lattice parameters. We recently demonstrated the possibility to generate in these materials a transient molecular and material transformation towards high spin multiplicity by using femtosecond laser irradiation of the LS phase[10,11].

In the monoclinic polymorph, a sequence of physical processes was evidenced by using ultrafast optical and x-ray techniques[10], otherwise hidden in the time domain. In a first step occurring at the molecular level, the LMCT to HS relaxation cascade occurs within 300 fs. In a second step, unit cell expansion occurs within 100 ns. In a third step, heating effects generate an additional thermal population of the HS state. Finally, the recovery to the thermal equilibrium occurs within few ms[28].

Here we present new results of ultrafast optical spectroscopy and X-ray diffraction in the 100 fs–10 ms time window for both polymorphs. Our results show that the first step is localized at the molecular level, with no indication of a cooperative response. The elastic step is also demonstrated to be sample dependent in terms of size and shape. The transient state is finally reached within ≈10–100 μs, where heating and elastic effects are relaxed. The present comparison of both polymorphs shows at a quantitative level that the main molecular LS to HS transformation effect resulting from the laser irradiation is not the purely photoinduced contribution which takes place at the early stage. A complex dynamics results from the energy deposition in the crystal, driving its macroscopic scale response within an out-of-equilibrium process that extends up to tenths of μs. It is this out-of-equilibrium dynamics which induces the most important molecular conversion from LS to HS states.

3 Methods

3.1 Ultrafast optical spectroscopy

The ultrafast dynamics of the photo-response of the [(TPA)Fe(TCC)]PF_6 polymorphs to 45 fs laser excitation were investigated by time-resolved optical experiments. We used typical photon densities up to 100 μJ/mm^2, *i.e.* below the damage value found to be around 300 μJ/mm^2. Experiments were performed by using a stroboscopic pump-probe method[10]. The light pulses generated by an amplifier at 1 kHz were split in pump and probe beams. Crystals were excited with near IR pulses (800 nm) in the vicinity of the absorption band (LMCT) of LS species. An optical parametric amplifier (OPA) was used for generating the 600 nm probing light, the wavelength we identified as most sensitive to the spin crossover for both polymorphs in the VIS range (Fig. 1). Pump and probe light used were polarized along the long crystal axis **a**. We used transmission geometry for probing the response of crystals of typically 200×100 $μm^2$ size. The pump-probe time resolution was ≈80 fs. Light was propagating along the **b** crystal axis, corresponding to the thickness of the crystals, which was in the 5–15 μm range.

This thickness, is approaching the laser penetration depth of the pump light for both polymorphs (3–5 μm @ 800 nm) and strikes a good compromise for maximizing the number of photo-excited molecules in the probed bulk. A phase sensitive detection set-up (lock-in amplifier Stanford) was used, in which the pumping rate is halved to 500 Hz with an optical chopper also phase-locked to the reference laser frequency. The earliest steps of the process, from 100 femtoseconds to 1 nanosecond, were monitored using a delay line. Longer delays between pump and probe were generated electronically by using a second amplifier seeded by the same oscillator. Pump and probe pulses were then delayed by triggering the Pockels cells of the second amplifier, and its Q-switch if necessary so that the pulses from the RF train are trapped and amplified later than those trapped in the first amplifier. By coupling this method in the same experiment with the femtosecond-resolved one, we can track the dynamical response to a laser excitation pump from 10s fs to ms by keeping the time resolution to ≈100 fs.

3.2 100 ps resolved x-ray diffraction

Time-resolved X-ray diffraction experiments were performed at the Biocars beamline at the APS synchrotron[29]. It is one of the beamlines[5,30–32] at synchrotrons allowing time-resolved diffraction studies at 100 ps resolution. X-ray pulses were selected by a fast chopper. X-ray diffraction data were collected for both polymorphs at 15 keV with a MAR-CCD detector and varying delays dt between the laser pump and the probe. For measuring the time dependence of the lattice parameters, partial data collections with at each delay 60 frames with 10 s exposure at 1° steps of the diffractometer φ axis. The plate shape crystals of were aligned perpendicular to this axis. The laser beam was incident along the φ rotation axis, and was circularly polarized to avoid any laser polarization dependence with respect to crystal rotation. We used typical excitation densities of 150 μJ/mm^2, with a laser beam diameter of ≈500 μm (FWHM), i.e. more than twice the samples sizes for an homogeneous excitation. The unit cell parameters and data reduction were obtained with CrysAlis software[33].

To evaluate the structural reorganization on spin cross-over, more complete data were accumulated for the monoclinic polymorph in a sequence consisting in measuring the diffraction pattern at every 1° oscillation for each time delay (−1 ns, 500 ps & 50 μs). We could only use the 220 first frames of these data collections because of subsequent deterioration of the crystal. The resulting intensities were averaged over repeated and symmetry-equivalent measurements with SORTAV[34]. Details of SORTAV merging and data filtering are listed in Table S1 of the supporting material. The structural changes were analysed with the LASER program.[35]

Least-squares analysis was only performed for data collected on the monoclinic form at the 50 μs time delay, since the number of reflections at the 500 ps time point was insufficient for this procedure. However, both the 500 ps and the 50 μs data were used for the calculation of photodifference maps using the −1 ns dataset as reference state as described further below.

At 50 μs, the structure of the excited state[36,37] was refined based on the response ratios η(hkl), defined as:

$$\eta(\mathrm{hkl})=(I_{50\mu s}(\mathrm{hkl})-I_{-1\mathrm{ns}}(\mathrm{hkl}))/I_{-1\mathrm{ns}}(\mathrm{hkl})=R(\mathrm{hkl})-1,$$

where $I_{50\mu s}(\mathrm{hkl})$ represents the intensities of the data collected 50 μs after laser excitation, and $I_{-1\mathrm{ns}}(\mathrm{hkl})$ the intensities of the data at the negative time delay −1 ns, *i.e.* with X-ray pulses probing the sample 1ns before the laser pulse excitation. R(hkl) is the ratio $I_{50\mu s}(\mathrm{hkl})/I_{-1\mathrm{ns}}(\mathrm{hkl})$. LASER assumes a random spatial distribution of the excited state species with the corresponding structure factor expression[38]:

$$F_{50\mu s}(hkl)=(1-P)\times F_{50\mu s,GS}(hkl)+P\times F_{50\mu s,ES}(hkl)$$

where GS and ES refer to the ground and excited states and P is the fraction of photo-converted molecules. In the refinement procedure the structure factor of the ground state was taken as the one measured at negative delays:

$$F_{-1ns}(hkl)=F_{50\mu s,GS}(hkl).$$

The ground state position of the Fe1 atom was used as the starting point of the excited state Fe1E atom. The excited state was defined as 5 rigid bodies, as further described in Fig. 2. Rigid bodies were allowed to rotate on their anchor atom, Fe1E and translate independent of the anchor atom. The positions of the ground state molecule and PF_6^- ion were kept fixed. The starting value of thermal factor, k_B, was estimated from the photo-Wilson plot. The ratio-agreement factor R_R[39] was used to compare observed and calculated ratios:

$$R_R=\frac{\sum_{hkl}|R_{obs}(hkl)-R_{calc}(hkl)|}{\sum_{hkl}R_{obs}(hkl)}$$

The final agreement obtained for 50 μs data set is R_R = 9.63%. A list of refinement details is given in table S2 of the supporting material. The molecular geometry from this LASER refinement was also used to estimate the excited state population of the 500 ps data, based on the 500 ps R_R factor changes on varying the population, as shown in Fig. S2 of the supporting information.

4 Results

4.1 Ultrafast dynamics studied by optical spectroscopy

The time dependent variation of optical transmission (ΔT) at 600 nm between negative and positive delays following fs laser excitation at 800 nm is shown in Fig. 3 for each polymorph. As the transmission varies in opposite directions for the two polymorphs between LS and HS states, −ΔT is plotted for the orthorhombic form in such a way that the positive signal at long delay corresponds to the formation of HS states. In this way it is easier to compare both polymorphs. Data were measured in the LS phase at 180 K for 40 μJ/mm^2 excitation density (≈2 photons/100 molecules). A transient absorption peak appears for both polymorphs as transmission decreases within the 80 fs time resolution. This is due to a Ligand-to-Metal Charge-Transfer state (LMCT state). It is followed by a variation of ΔT characteristic of an exponential-like population of the HS state, which is fed from the LMCT state with τ≈300 fs time constant. The initial steps of LS-HS conversion in solids is therefore as fast as the one observed for similar spin-crossover molecules in solution[40–45]. The evolution of the response with laser fluence measured on the monoclinic polymorph is presented in Fig. 4. It only shows a linear response and therefore no threshold or cooperative effect is detected here. This linear response on ultrashort time-scale is also a clear indication that the early events in the photoinduced spin-state switching occurs locally at the molecular level in this non-cooperative sample.

4.2 Optical spectroscopy studies of ns-ms dynamics

The photoconverted HS fraction on the picosecond plateau is estimated to ≈0.5–1%, and it extends as such up to a few ns as observed in Fig. 5. The main difference between this study

and the case of photoinduced spin-crossover dynamics for molecules in solution is that in the latter case the relaxation of photo-excited molecules occurs within ns as the molecules cool down by heat exchange with the solvent[40–45]. In the present case, we do not observe relaxation of photoinduced molecular switching but an additional conversion in the active crystal medium. An abrupt increase of the response occurs after few ns, and continues until ≈ 1 μs. After that, a third step is observed, especially in the data for the monoclinic polymorph, around 10 μs after laser excitation. This last stage was clearly demonstrated to be associated with a thermal heating effect in previous picosecond X-ray diffraction studies[10]. However these were limited in the number of measurements in this time domain and did not reveal structural signature on ns delay.

The ns step is clearly observed in the current time-resolved X-ray analysis performed at Biocars, making it possible to assign this ns step to elastic effects as lattice expansion occurs at this time. The transmission changes plotted in Fig. 5 were compared and normalized to values measured during the thermal conversion (Fig. 1), so that the scales correspond approximately to the HS fraction X_{HS}. We estimate from optical data that this jump corresponds to an increase of the fraction of HS molecules by a factor of ~5–10 compared to the intramolecular step which occurs within 300 fs, as the converted fraction of HS molecules approaches 5–10% on μs delays.

This higher conversion rate for the orthorhombic polymorph might be related to the smaller thickness of the sample used (≈7 μm) compared to the monoclinic one (≈15 μm), making it possible to have a better matching between the sample thickness and the laser penetration depth (reaching for both polymorphs 3–5 μm).

Finally, both polymorphs recover the initial state existing prior to laser excitation on a ms time scale, in good agreement with time-resolved studies of the lifetime of the transient photoexcited state[30].

4.3 Elastic and heating effects probed by X-ray diffraction

The structural reorganization associated with the swelling of the molecules and lattice heating induces expansion of the crystal volume. It can be easily detected by time-resolved X-ray diffraction, as shown in Fig. 6 for the monoclinic polymorph. From these results, we observe that the first stage of the transformation detected by femtosecond optical spectroscopy takes place in a crystal with a constant lattice. Indeed, it takes time for cell deformation to propagate and these elastic effects therefore occur at the speed of sound. We observe an abrupt increase of the lattice parameter **b** around 4 ns, as indicated in Fig 6 & 7 and a second slower step in the 1 μs–100 μs range.

This response is anisotropic since the increase of the lattice parameter **a** is slower and takes few tenths of ns. It is followed by slower heating effect in the 100 ns–100 μs range[10, 14]. The earlier investigations provided a more accurate evolution of **a** than the current study, because a different diffraction geometry was used. The lattice expansion is clearly governed by propagating effects and the timescale is therefore sample dependent. This is illustrated in Fig. 7, which compares the lattice expansion of two crystals of the monoclinic polymorph, and shows the time dependence of the lattice parameters $\mathbf{b_1}$ for sample 1 (≈20 μm thick) and $\mathbf{b_2}$ for sample 2 (≈7 μm thick). A faster expansion of lattice parameter **b** is observed when the thickness (corresponding to **b** axis) of the crystal plate is reduced. It is expected that the expansion time varies linearly with the sample thickness, in good agreement with expansion time of 5 ns (respectively 1.5 ns) for the 20 μm (resp. 7μm) thick crystal presented in Fig. 7. Similar responses were observed for the orthorhombic polymorph but with a too limited number of data to allow detailed conclusions.

Since conversion related to heat diffusion effects is more rapidly activated when the size is small, the excitation of crystals of anisotropic shape induces in the time domain anisotropic deformations. This can be observed by deformation of the Bragg peaks in the reciprocal lattice. Fig. 8 shows reconstruction of different reciprocal planes before laser excitation (−1 ns) and after laser excitation when the effect is maximum (10 μs) measured on a 200×200×7 μm^3 single crystal of the orthorhombic form. In the (**a***,**c***) plane no significant deformation is observed, whereas in the (**a***,**b***) and (**b***,**c***) planes an important broadening of the Bragg peaks is observed.

With the present X-ray diffraction measurements, this recovery to equilibrium can be observed by the relaxation of the lattice parameters **a** and **b** plotted in Fig. 9 for the monoclinic polymorph. This kinetics is governed by heat exchange with the sample environment. Compared to previous studies performed with 1 kHz repetition rate, the present study, performed at 40 Hz, allows precise determination of the recovery time of ≈ 8 ms.

4.4 Structural analysis of the molecular reorganization

The photodifference maps of type II ($F_{obs}^{dt>0} - F_{obs}^{-1ns}$) based on independent reflections with $I/\sigma(I) > 4$, calculated at isosurfaces of $\pm 0.14 eÅ^{-3}$ and $0.46 eÅ^{-3}$ respectively for dt = 500 ps and 50μs are shown in Fig. 10. These two maps show significant changes in the electron density on excitation. The molecular response on excitation at 500 ps is illustrated by the sideward shift of the electron density of the Fe1 atom towards O2 (Fig. 10a). This shift is even more pronounced at 50 μs time delay (Fig. 10b). At this delay, the excited state population should be significantly higher in view of the optical data presented in Fig. 5. Additionally an increase of the Fe-N distances is observed (Tab. 1).

The estimated population of the excited state at 500 ps is in the 1.5% – 2% range. LASER refinement of 50 μs data indicates a much larger excitation percentage of 10.5 (16) %. The increase of excited state population with longer time delay due to the temperature increase agrees also well with the signal seen on photodifference maps, associated with a larger change of the average structure. The molecular geometry of the excited state at 50 μs is compared in table 1 with the one of the ground state measured at −1 ns delay. Although the standard deviations are large, all changes in the Fe-N bond lengths are positive, as expected. This is a result of a significant shifts of the iron by 0.17(2)Å and of the two oxygen atoms.

Discussion

The photoinduced switching dynamics in both spin-crossover materials can present different consecutive steps. Just after the femtosecond laser excitation, the LMCT state generated at the molecular level relaxes towards the metastable HS molecular state, illustrated by dots at dt = 0 ps in scheme 1.

This process occurs with a typical 300 fs time-constant corresponding well to time-scales reported for spin crossover molecules in solution[40–45]. The related molecular swelling and the lattice heating induce an internal pressure and generate a propagating nonlinear wave resulting in crystal expansion during the next step. Since the crystals used have anisotropic shapes, the elastic stress propagation is faster along the thickness (≈20 μm within few ns) than along the perpendicular directions (200 μm within ≈ 50 ns). Such a pressure front induces an over-compressed region followed by a depression, which will favour switching from LS to HS states. During this elastic expansion in the 2ns–100ns time window, the fraction of HS molecule increases.

The optical energy absorbed at the molecular level is much higher than the thermal energy difference between LS and HS states. This energy is mainly redistributed as heat in the crystal, resulting in a global warming. The temperature homogenization is reached within 10 μs at the macroscopic level, leading to an increase of the average temperature. This heating and the associated additional conversion to HS states result both in another lattice expansion within 100 ns–100 μs.

However, the gradient of deposited optical energy over the sample thickness (**b** axis in scheme 1) induces a temperature gradient in the crystal thickness. This gradient of temperature gives rise to an inhomogeneous distribution of unit cell volume over the sample thickness. This gradient of unit cell parameter over the **b** axis induces a deformation of the Bragg reflections in the (**b***,**a***) and (**b***,**c***) reciprocal planes, but not in the (**a***,**c***) planes (Fig. 9). The unit cell gradient of lattice parameters **a** or **c** over the thickness corresponding to the **b** axis should give rise to a radial broadening of the peaks in the (**a***,**c***) plane. But this expected broadening, which can be estimated by the corresponding variation of lattice parameters in Fig. 6, is smaller than the HWHM of the Bragg peaks and therefore difficult to observe. The deformation of the peaks is therefore very likely associated with the inhomogeneous distribution of the lattice parameters over the sample thickness, as the crystal is not equilibrated, which should induce a crystal deformation.

Within 50 μs, temperature is homogeneous in the sample and the reciprocal lattice recovers its initial shape. This increase of temperature results in a higher population of the HS fraction (thermally activated) in the transient equilibrated state.

The elastic and thermal steps clearly underline the active role of the crystal medium, made of switchable molecules, mediating a self-amplification process. This type of phenomena cannot exist for molecules in solution, as the solvent is mainly passive. The interaction of the photo-excited molecule with the surrounding media only results in transfer of excess energy. In the active crystalline medium studied here, this energy transfer, which takes different forms (elastic and thermal), is at the origin of additional switching activation across the crystal.

Conclusions

The present results underline the very good correlation between time-resolved optical data (mainly sensitive to the electronic molecular state) and X-ray data (sensitive to structural deformation) in systems where electronic and structural degrees of freedom are strongly coupled. Our data show that a macroscopic system made of bistable molecules can be switched on ultra-short timescale, and as so represents a first test for crossing the border between femtochemistry at the molecular scale and femtoswitching at the material scale.

However, in the present systems, our data also clearly give evidence that macroscopic descriptions are required in fast transformation of matter driven by light irradiation. It is necessary here to take into account the shock-wave driven transformation or heating effect for example. By comparing two solids made of the same molecules, we can draw general conclusion on the occurrence of different steps, resulting from different stimuli driven by light: photo-switching, elasto-switching and thermo-switching. These last two effects, which finally prevail over the purely photoinduced effect observed on the femtosecond time scale may be limited by chemical engineering if in future material the elastic effects can be diminished, with less deformable molecules or by introducing absorbers in the crystal, or/ and reducing the heating effects with HS states unreachable at high temperature. The detailed crystallography analysis presented here and elsewhere also opens the way towards

femtosecond crystallography[47], which will hopefully be performed on the new generation of femtosecond x-ray sources[48].

Supplementary Material

Refer to Web version on PubMed Central for supplementary material.

Acknowledgments

This work was supported by the Institut Universitaire de France, Rennes Métropole, Région Bretagne (CREATE Ultimate 4146), the ANR (09-BLAN-0212) and ACI (JC E. Collet), Europe (FEDER) and by the US National Science Foundation (CHE0843922). Use of the Advanced Photon Source was supported by the U.S. Department of Energy, Basic Energy Sciences, Office of Science, under Contract No. DE-AC02-06CH11357. Use of the BioCARS Sector 14 was supported by the National Institutes of Health, National Center for Research Resources, under grant number RR007707

Notes and references

1. Koshihara S, Kuwata-Gonokami M. J. Phys. Soc. Jpn. 2006; 75 011001.
2. Chollet M, Guerin L, Uchida N, Fuhaya S, Shimoda H, Ishikawa T, Matsuda K, Hasegawa T, Ota A, Yamochi H, Saito G, Tazaki R, Adachi S, Koshihara S. Science. 2005; 307:86. [PubMed: 15637272]
3. Okimoto Y, Miyata T, Endo MS, Kurashima M, Onda K, Ishikawa T, Koshihara S, Lorenc M, Collet E, Cailleau H, Arima T. Phys. Rev. B. 2011; 84:121102.
4. Ishikawa T, Fukazawa N, Matsubara Y, Nakajima R, Onda K, Okimoto Y, Koshihara S, Lorenc M, Collet E, Tamura M, Kato R. Physical Review B. 2009; 80:115108.
5. Collet E, Lemée-Cailleau M-H, Buron-Le Cointe M, Cailleau H, Wulff M, Luty T, Koshihara S-Y, Meyer M, Toupet L, Rabiller P, Techert S. Science. 2003; 300:612–615. [PubMed: 12714737]
6. Guérin L, Collet E, Lemée-Cailleau MH, Buron M, Cailleau H, Plech A, Wulff M, Koshihara S, Luty T. Chem. Phys. 2004; 299:163.
7. Bonhommeau S, Molnar G, Galet A, Zwick A, Real J-A, McGarvey JJ, Bousseksou A. Angew. Chem. Int. Ed. 2005; 44:4069.
8. Fouché O, Degert J, Jonusauskas G, Daro N, Létard J-F, Freysz E. Phys. Chem. Chem. Phys. 2010; 12:3044. [PubMed: 20449397]
9. Galle G, Degert J, Mauriac C, Etrillard C, Letard JF, Freysz E. Chem. Phys. Lett. 2010; 500:18–22.
10. Lorenc M, Hébert J, Moisan N, Trzop E, Servol M, Buron-LeCointe M, Cailleau H, Boillot M-L, Pontecorvo E, Wulff M, Koshihara S, Collet E. Phys. Rev. Lett. 2009; 103 028301.
11. Moisan N, Servol M, Lorenc M, Tissot A, Boillot M-L, Cailleau H, Koshihara S, Collet E. C. R. Chimie. 2008; 11:1235.
12. Collet E. Acta Cryst. A. 2010; 66:133. [PubMed: 20164636]
13. Zewail AH. Angew. Chem. Int. Ed. 2000; 39:2586–2631.
14. Cailleau H, Lorenc M, Guérin L, Servol M, Collet E, Buron-LeCointe M. Acta Cryst. A. 2010; 66:189. [PubMed: 20164642]
15. Goujon A, Varret F, Boukheddaden K, Chong C, Jeftic J, Garcia Y, Naik AD, Ameline JC, Collet E. Inorganica Chimica Acta. 2008; 361:4055–4064.
16. Bréfuel N, Watanabe H, Toupet L, Come J, Matsumoto N, Collet E, Tanaka K, Tuchagues J-P. Angew. Chem. Int. Ed. 2009; 48:9304–9307.
17. Decurtins S, Gütlich P, Köhler CP, Spiering H, Hauser A. Chem. Phys. Lett. 1984; 105:1.
18. Létard JF, Capes L, Chastanet G, Moliner N, Létard S, Real JA, Kahn O. Chem. Phys. Lett. 1999; 313:115.
19. Létard JF, Guionneau P, Rabardel L, Howard JAK, Goeta AE, Chasseau D, Kahn O. Inorg. Chem. 1998; 37:4432. [PubMed: 11670580]
20. Gütlich P, Goodwin HA. Top. Curr. Chem. 2004; 233:234–235.
21. Collet E, Lorenc M, Buron-LeCointe M, Cailleau H. Z. Krist. 2008; 223:272–282.

22. Sheu C-F, Chen S-M, Wang S-C, Lee G-H, Liu Y-H, Wang Y. Chem. Commun. 2009; 48:7512–7514.b) Shih CH, Cheu CF, Kato K, Sugimoto K, Kim J, Wang Y, Takata M. Dalton Trans. 2010; 39:9794–9800. [PubMed: 20830440]
23. Marchivie M, Guionneau P, Létard JF, Chasseau D. Acta Cryst. B. 2003; 59:479. [PubMed: 12947232]
24. Legrand V, Pillet S, Souhassou M, Lugan N, Lecomte C. J. Am. Chem. Soc. 2006; 128:13921–13931. [PubMed: 17044720]
25. Pillet S, Legrand V, Souhassou M, Lecomte C. Phys. Rev. B. 2006; 74:140101.
26. Collet E, Buron-LeCointe M, Cailleau H. J. Phys. Soc. Jpn. 2006; 75 011002.
27. Collet E, Boillot M-L, Hébert J, Moisan N, Servol M, Lorenc M, Toupet L, Buron-LeCointe M, Tissot A, Sainton J. Acta Cryst. B. 2009; 65:474. [PubMed: 19617683]
28. Enachescu C, Hauser A, Girerd J-J, Boillot M-L. Chem. Phys. Chem. 2006; 7:1127. [PubMed: 16586423]
29. Graber T, Anfinrud P, Brewer H, Chen Y-S, Cho H-S, Dashdorj N, Henning RW, Kosheleva I, Macha G, Meron M, Pahl R, Ren Z, Ruan S, Schotte F, Šrajer V, Viccaro PJ, Westferro F, Moffat K. J. Synchrotron Rad. 2011; 18:658–670.
30. Nozawa S, Adachi S, Takahashi J, Tazaki R, Guérin L, Daimon M, Tomita A, Sato T, Chollet M, Collet E, Cailleau H, Yamamoto S, Tsuchiya K, Shioya T, Sasaki H, Mori T, Ichiyanagi K, Sawa H, Kawata H, Koshihara S. J. Synchrotron Rad. 2007; 14:313–319.
31. Johnson SL, Beaud P, Milne CJ, Krasniqi FS, Zijlstra ES, Garcia ME, Kaiser M, Grolimund D, Abela R, Ingold G. Phys Rev Lett. 2008; 100:155501. [PubMed: 18518120]
32. Guérin LL, Hebert J, Buron-Le Cointe M, Adachi S, Koshihara S, Cailleau H, Collet E. Phys. Rev. Lett. 2010; 105:246101. [PubMed: 21231536]
33. CrysAlis RED, Version 1.171.26. Abingdon, Oxfordshire, England: Oxford Diffraction Ltd;
34. Blessing RH. J. Appl. Cryst. 1997; 30:421–426.
35. Vorontsov I, Pillet S, Kaminski R, Schmøkel MS, Coppens P. J. Appl. Cryst. 2010; 43:1129–1130.
36. Makal A, Trzop E, Sokolow J, Kalinowski J, Benedict J, Coppens P. Acta Cryst. A. 2011; 67:319–326. [PubMed: 21694470]
37. Coppens P, Benedict J, Messerschmidt M, Novozhilova I, Graber T, Chen Y-S, Vorontov I, Scheins S, Zheng S-L. Acta Cryst. A. 2010; 66:179–188. [PubMed: 20164641]
38. Vorontsov II, Coppens P. J. Synchr. Rad. 2005; 12:488–493.
39. Coppens P, Kamiński R, Schmøkel MS. Acta Cryst. A. 2010; 66:626–628. [PubMed: 20720326]
40. Gawelda W, Pham V-T, Benfatto M, Zaushitsyn Y, Kaiser M, Grolimund D, Johnson SL, Abela R, Hauser A, Bressler C, Chergui M. Phys. Rev. Lett. 2007; 98 057401.
41. Bressler C, Milne C, Pham V-T, El Nahhas A, van der Veen RM, Gawelda W, Johnson S, Beaud P, Grolimund D, Kaiser M, Borca CN, Ingold G, Abela R, Chergui M. Science. 2009; 323:489. [PubMed: 19074309]
42. Khalil M, Marcus MM, Smeigh AL, McCusker JK, Chong HHW, Schoenlein RW. J. Phys. Chem. A. 2006; 110:38. [PubMed: 16392837]
43. Brady C, McGarvey JJ, McCusker JK, Toftlund H, Hendrickson DN. Top. Curr. Chem. 2004; 235:1.
44. Cannizzo A, van Mourik F, Gawelda W, Zgrablic G, Bressler C, Chergui M. Angew. Chem. Int. Ed. 2006; 45:3174.
45. Tribollet J, Galle G, Jonusauskas G, Deldicque D, Tondusson M, Letard JF, Freysz E. Chem. Phys. Lett. 2011; 513:42–47.
46. Volkov, A.; Macchi, P.; Farrugia, LJ.; Gatti, C.; Mallinson, PR.; Richter, T.; Koritsanszky, T. Germany: Middle Tennessee State University, USA, Universita` di Milano and CNR-ISTM Milano, Italy, University of Glasgow, Scotland, State University of New York at Buffalo, USA, and Freie Universität Berlin; 2006. XD2006.
47. Collet E, Lorenc M, Cammarata M, Guérin L, Servol M, Tissot A, Boillot ML, Cailleau H, Buron-LeCointe M. Chem. Eur. J. in press.

48. Kirian RA, White TA, Holton JM, Chapman HN, Fromme P, Barty A, Lomb L, Aquila A, Maia FR, Martin AV, Fromme R, Wang X, Hunter MS, Schmidt KE, Spence JC. Acta Cryst. A. 2011; 67:131–140. [PubMed: 21325716]

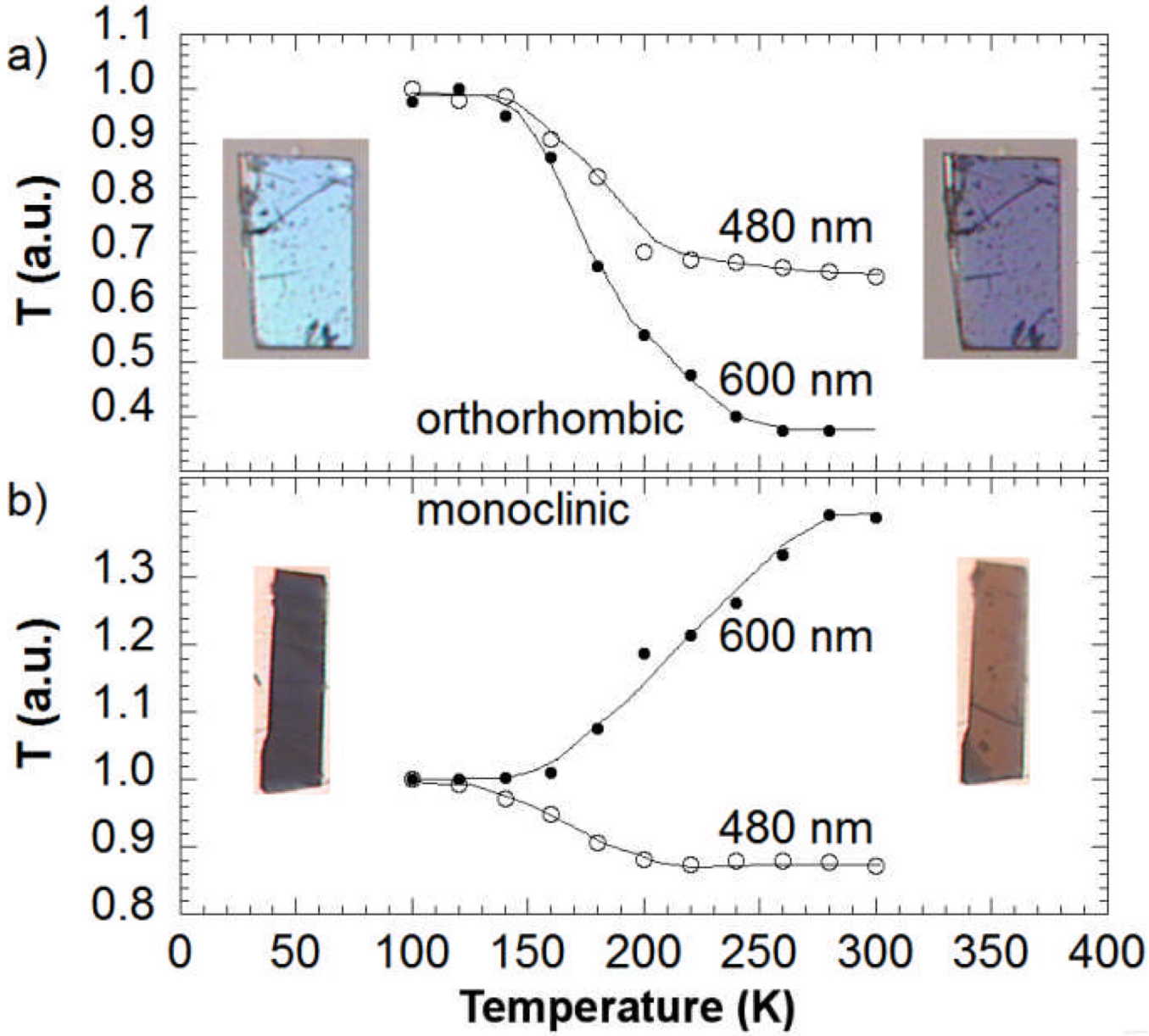

Fig. 1.

Temperature dependence of the optical transmission at 480 and 600 nm normalized to values at 100 K for the orthorhombic (a) and monoclinic (b) polymorphs. Measurements were performed with light polarized parallel to the long crystal axis **a**. Photographs were obtained at 50 and 350 K.

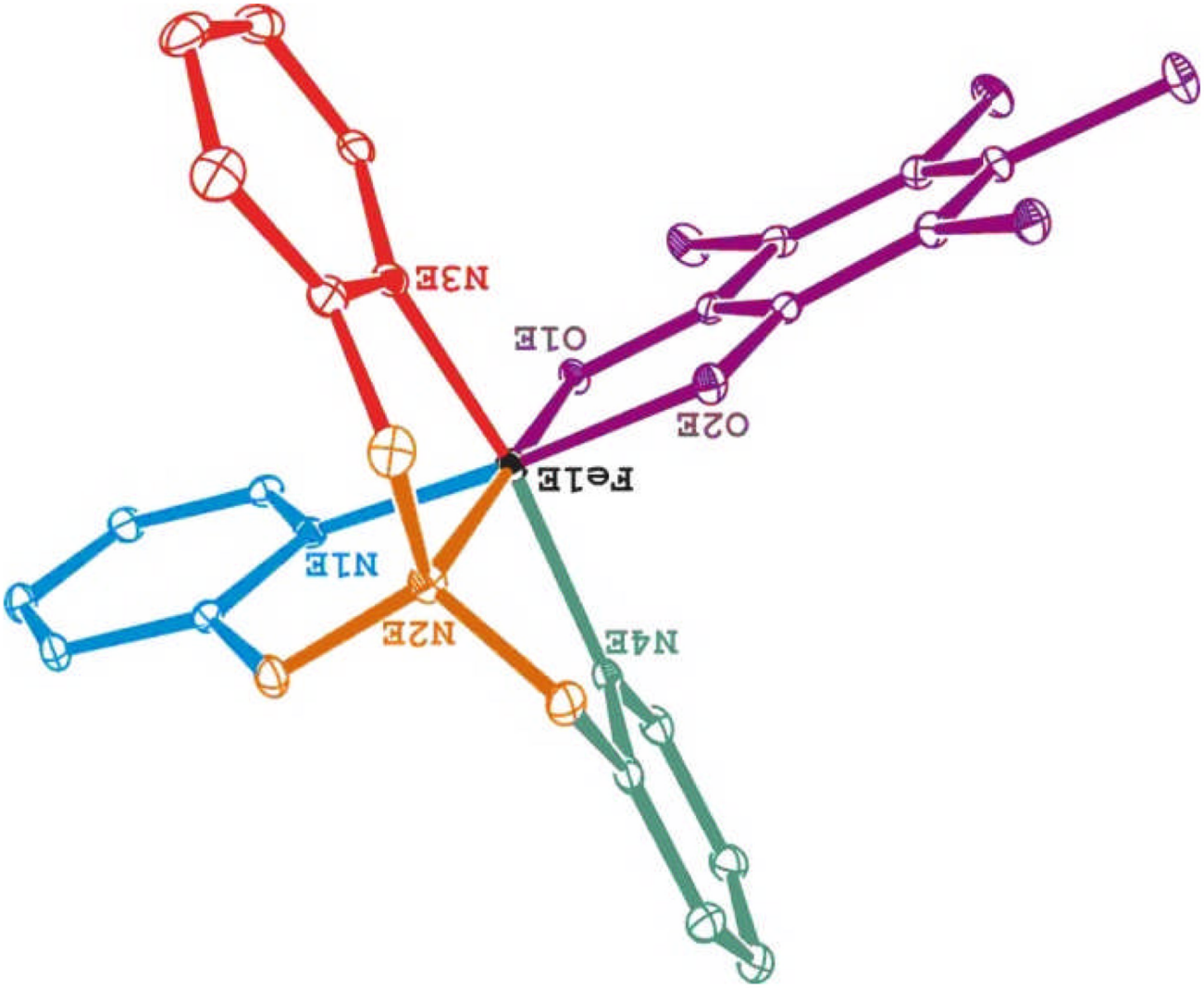

Fig. 2.

Structure of the [(TPA)$Fe^{(III)}$(TCC)] cation of both polymorphs and the rigid bodies' model used for the refining the structure of the excited state with the LASER refinement. The TCC ligand was treated as one rigid body (violet lines) whereas the TPA ligand was split into 4 parts (orange, red, blue and green lines represent each of the rigid fragments). The PF_6^- counter ion and hydrogen atoms are omitted for clarity.

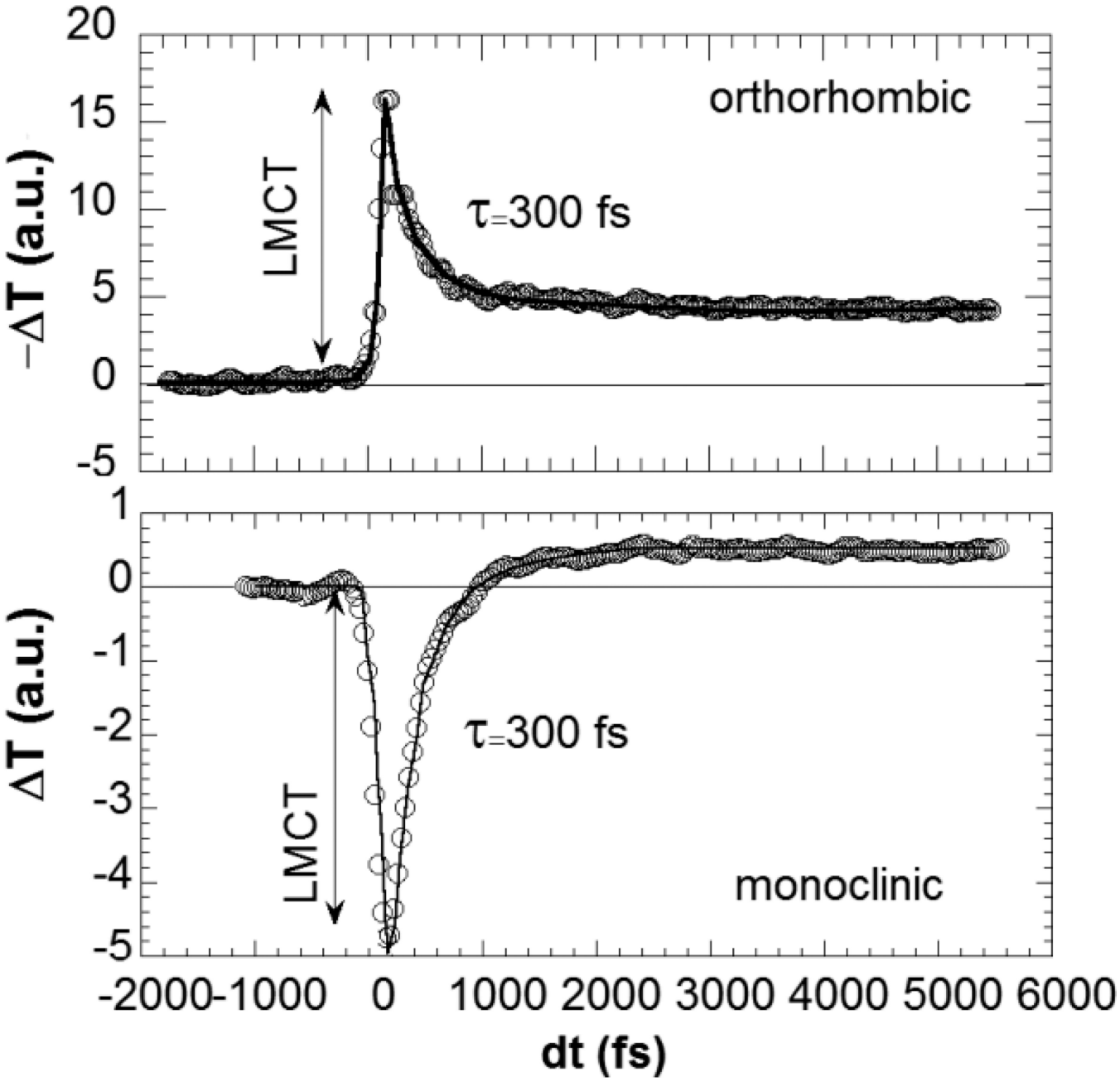

Fig. 3.
Time dependence of the variation of transmission in ultra-short scale −ΔT (orthorhombic) and ΔT (monoclinic) at 600 nm following femtosecond laser excitation at 800 nm.

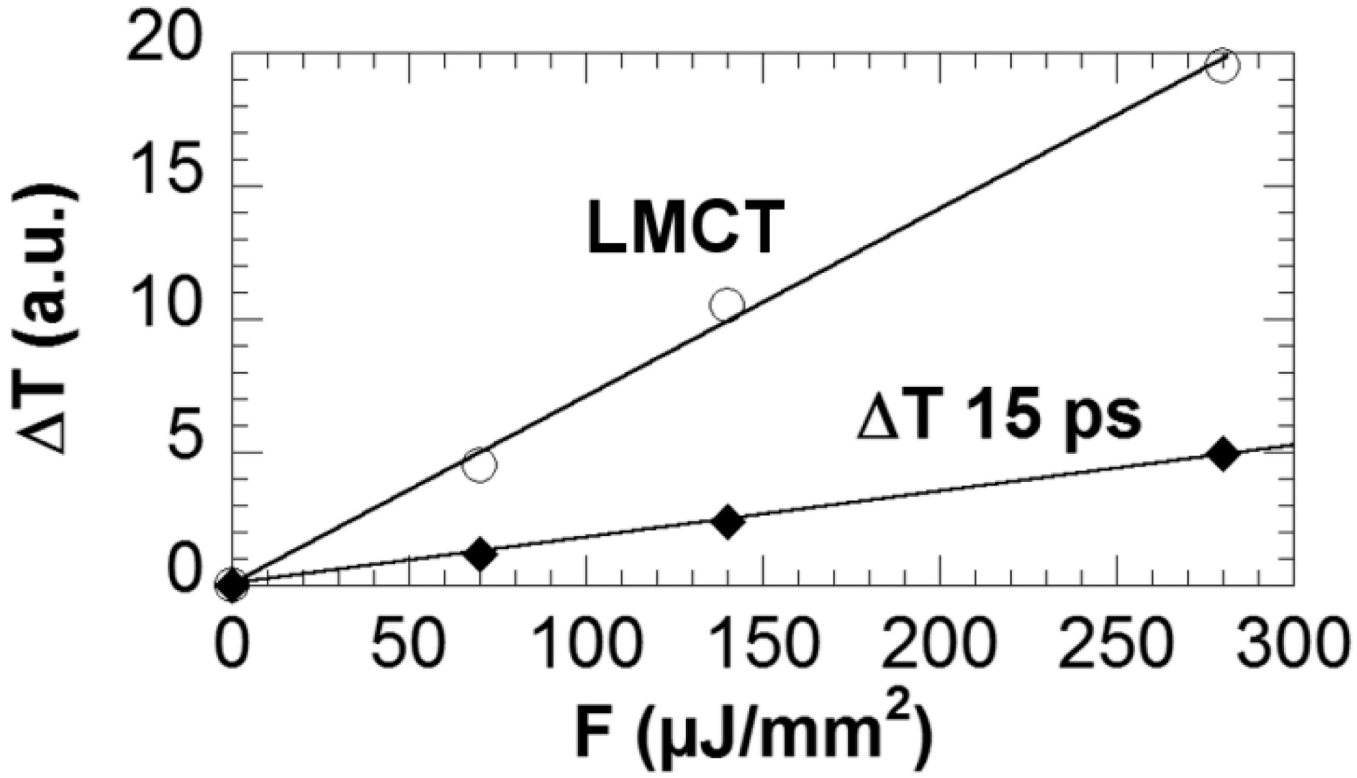

Fig. 4.
Fluence dependence of the photo-response on the LMCT peak and transmission variation at 15 ps (monoclinic polymorph).

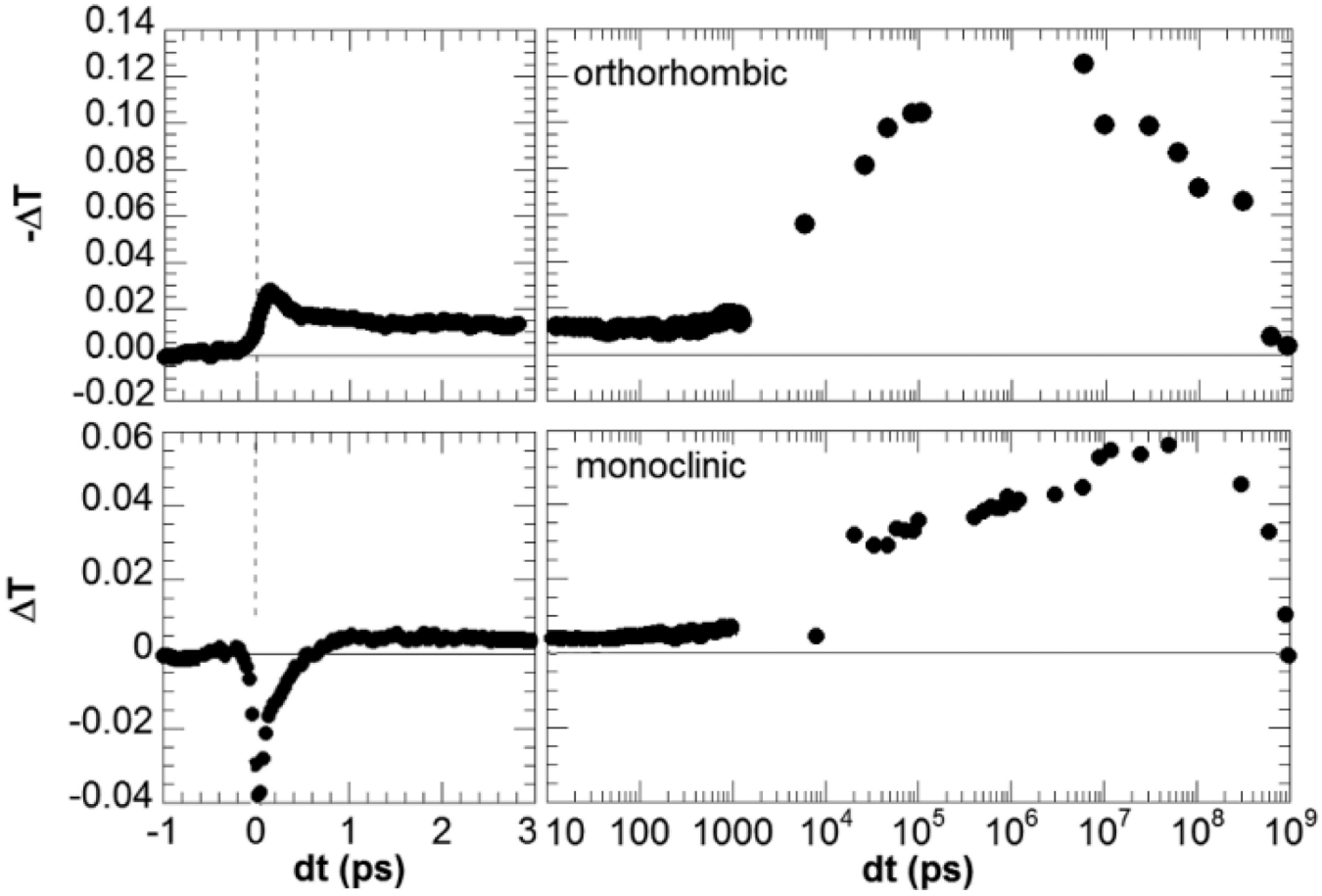

Fig. 5.
Time dependence of the variation of transmission over several temporal scales −ΔT (orthorhombic) and ΔT (monoclinic) at 600 nm following femtosecond laser excitation at 800 nm.

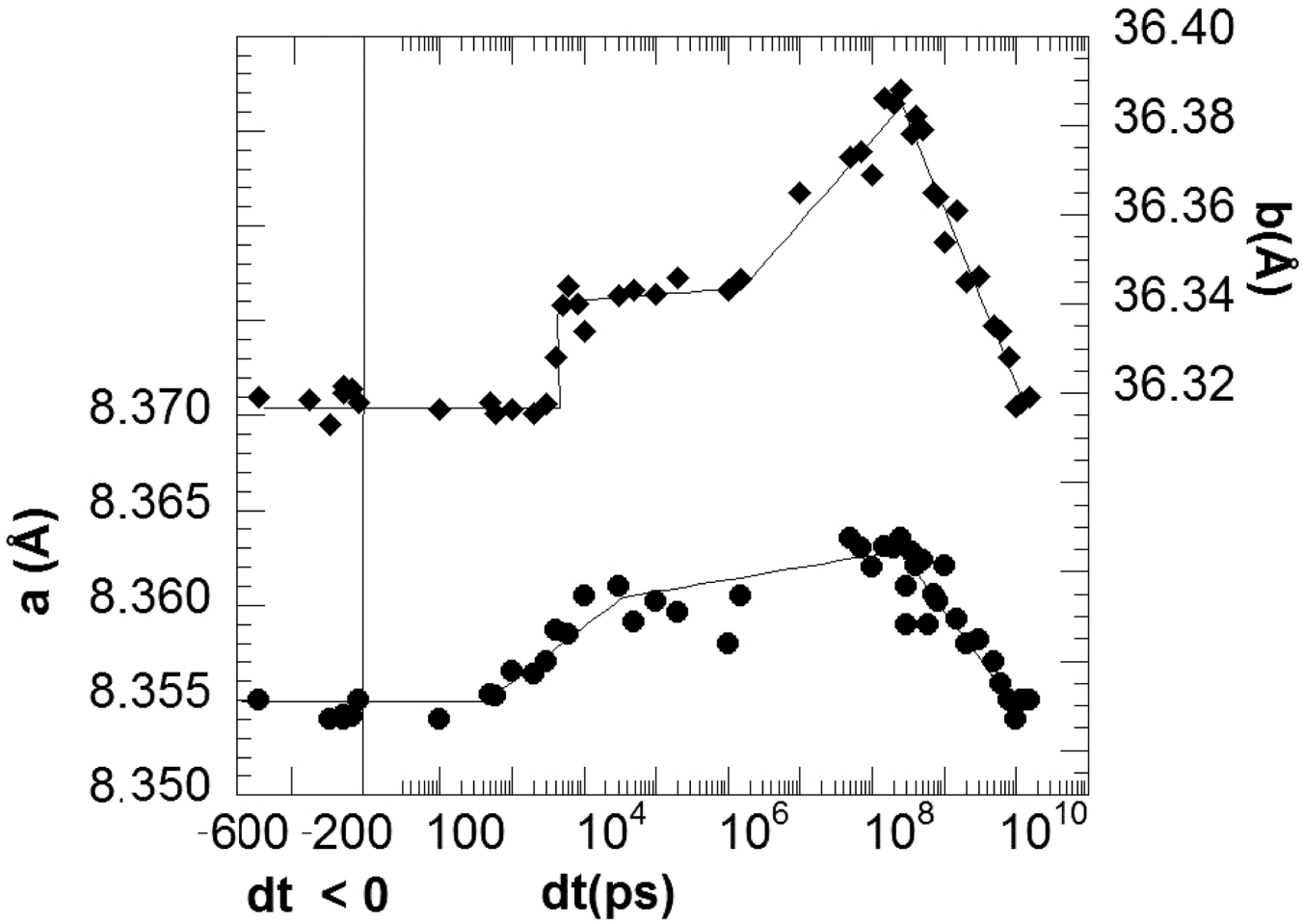

Fig. 6.
Time dependence of the lattice parameters **a** (●) and **b** (♦ sample thickness) measured on the monoclinic polymorph.

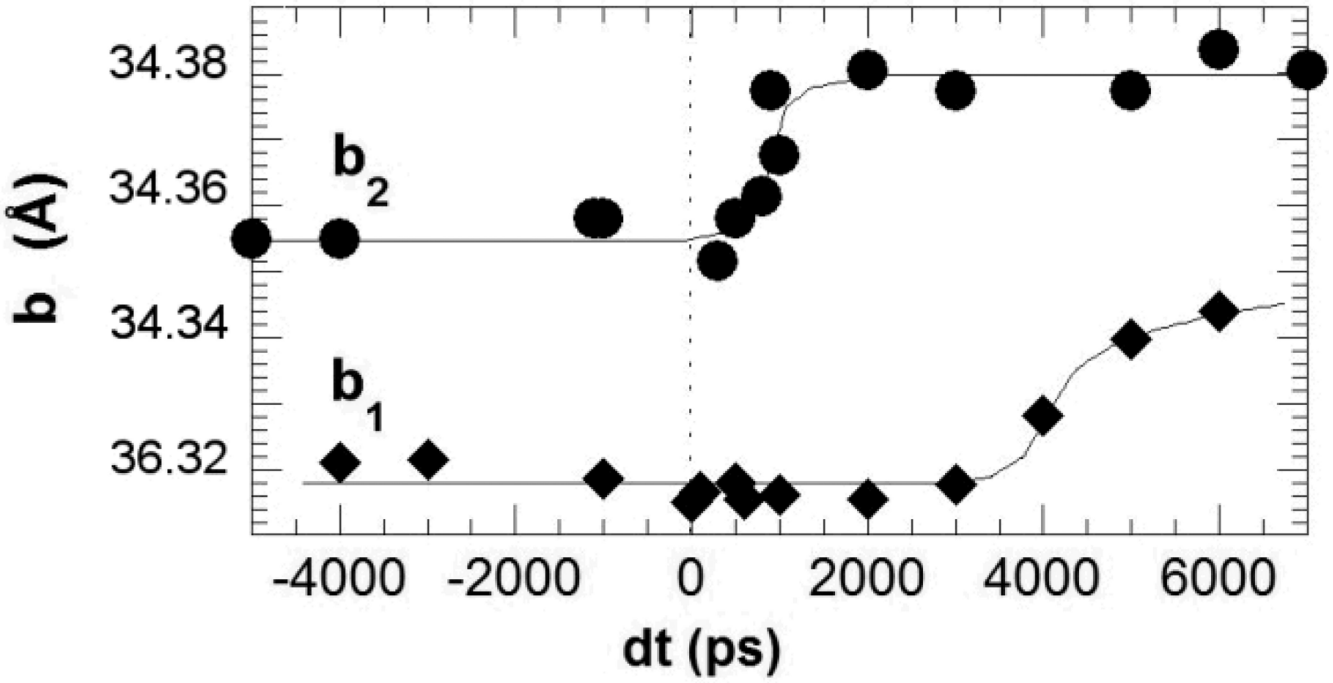

Fig. 7.

Time dependence of the lattice parameters b of 2 crystals of the monoclinic polymorph with 20 μm (b_1 ♦) and a 7 μm (b_2 ●) thickness. b_2 values are shifted for clarity.

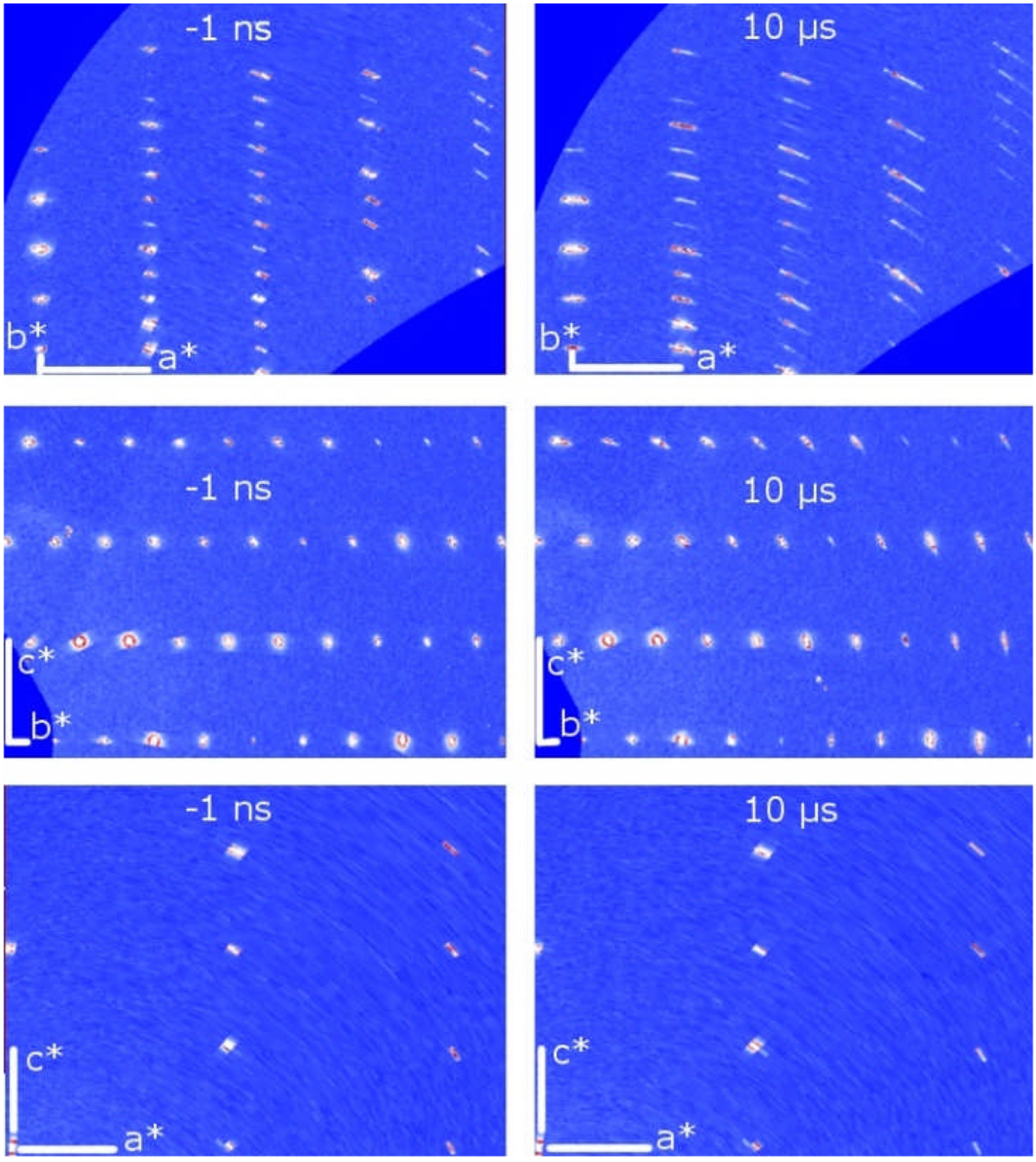

Fig. 8.
Evolution of the diffracted intensity from on the orthorhombic polymorph in the (a*,c*), (b*,c*) and (a*,b*) reciprocal planes, showing a deformation of the Bragg peaks between −1 ns and 10 µs.

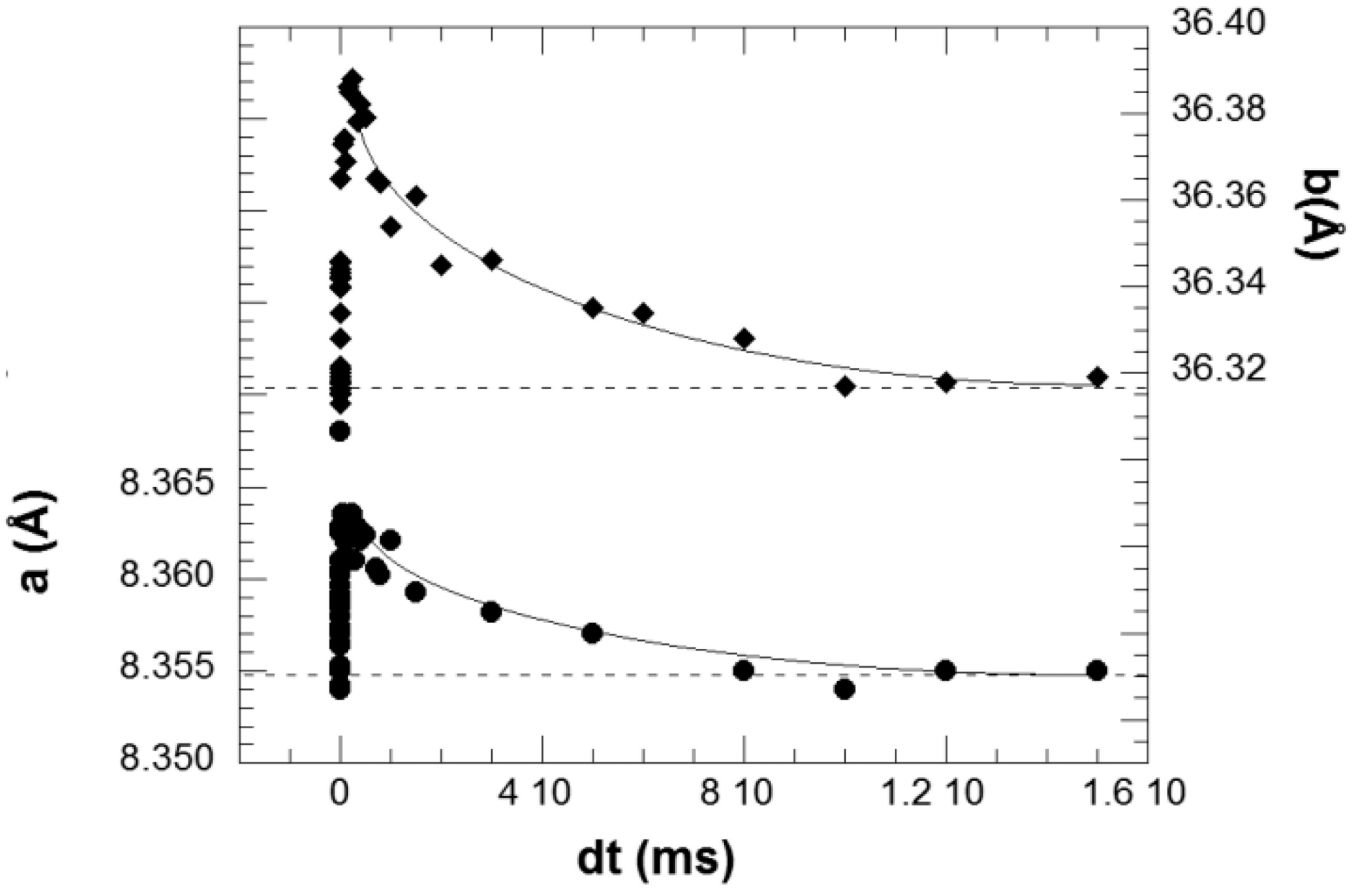

Fig. 9.
Time dependence of the lattice parameters a (●) and b (♦) in the ms window measured on the monoclinic polymorph.

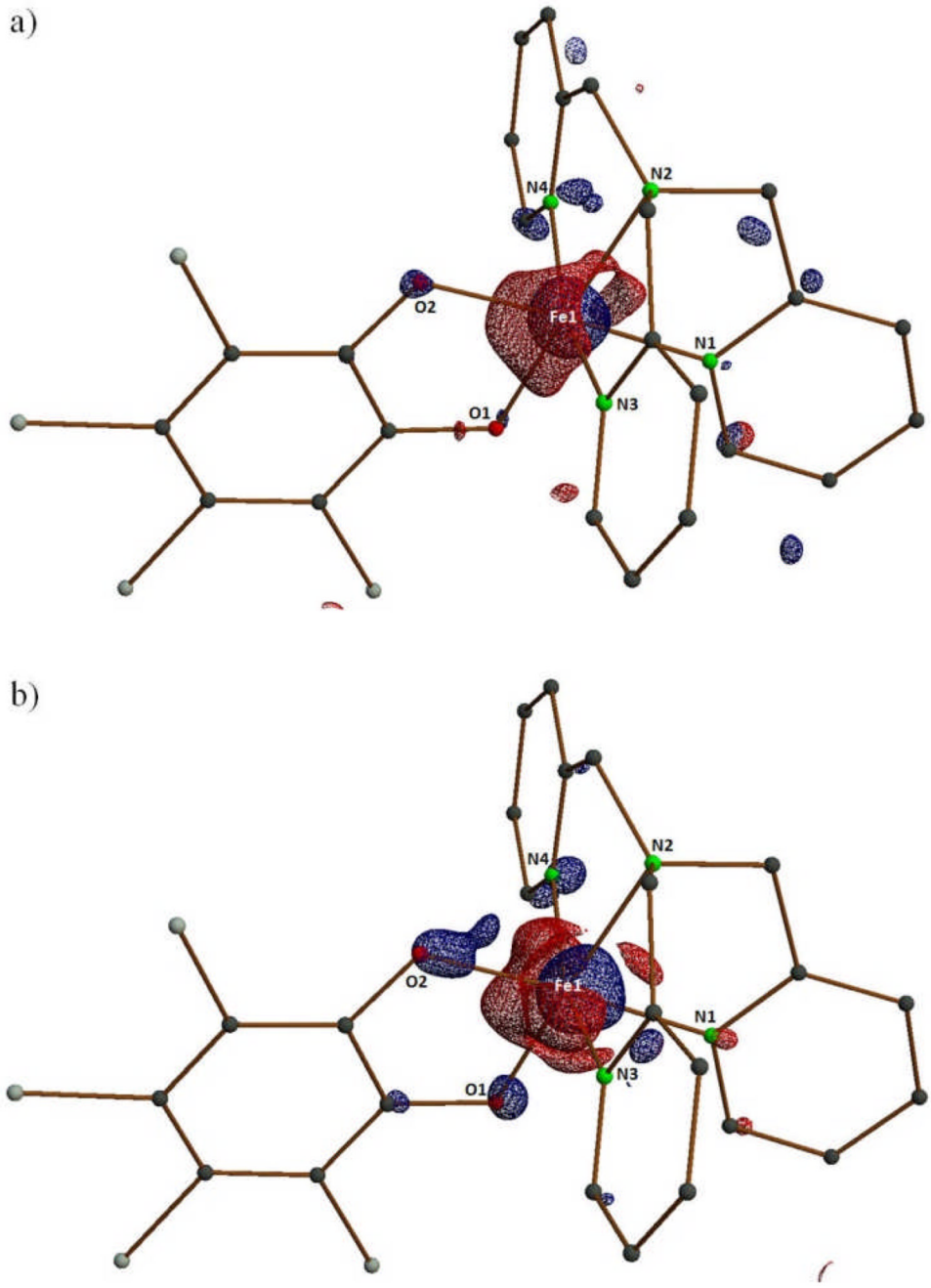

Fig. 10.

Photodifference maps obtained for the monoclinic polymorph with isosurfaces (red positive, blue negative) of (a) ±0.14eÅ^{-3} for the 500ps data and (b) ±0.46eÅ^{-3} for the 50μs data calculated with XDGRAPH of the XD program set[43]. The PF_6^- counter ion and hydrogen atoms are omitted for clarity.

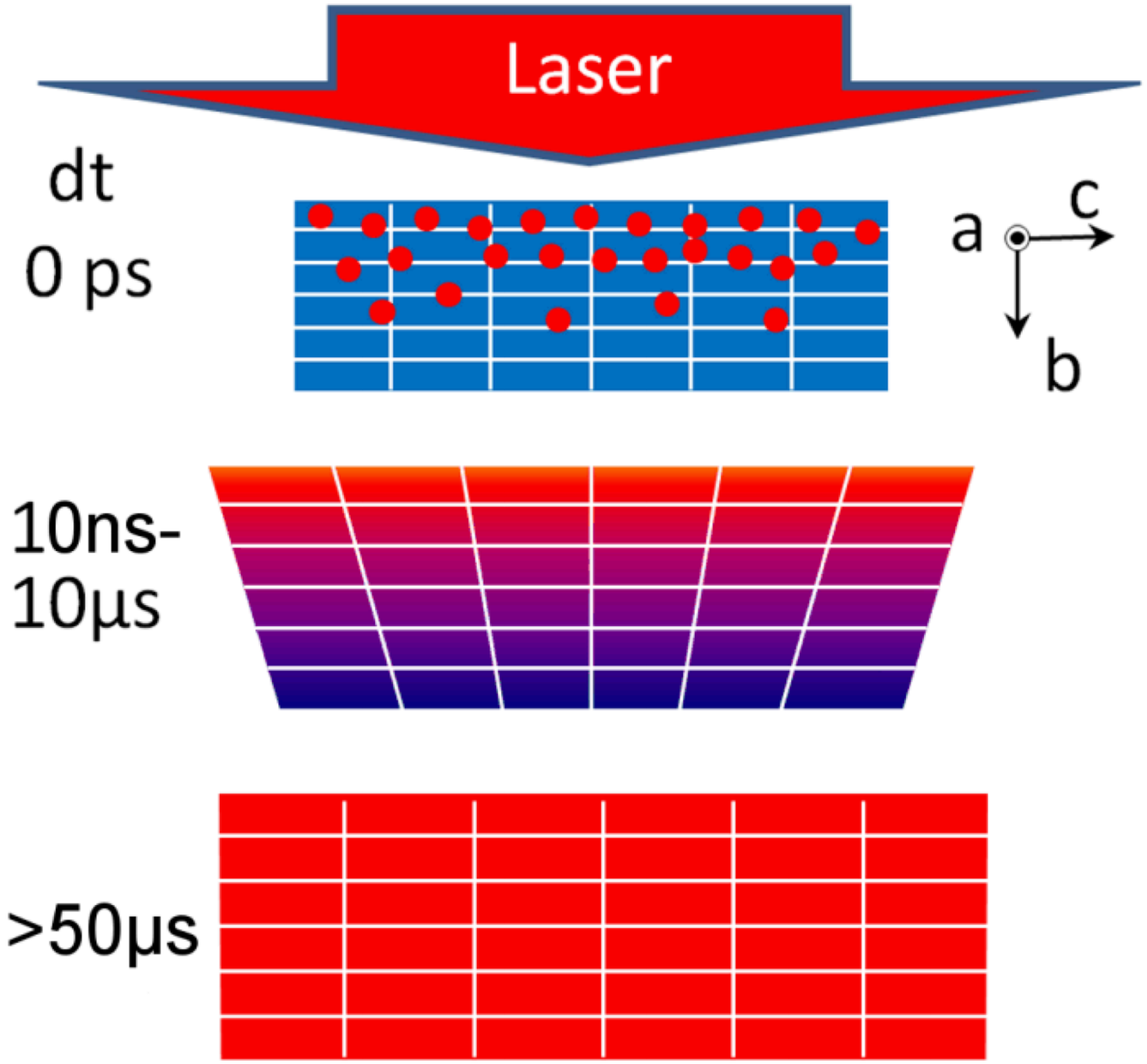

Scheme 1.

Schematic drawing of the dynamics. The laser deposits energy on photo-excited molecules (dots) of the crystal at dt = 0 ps. The gradient of deposited energy results in an inhomogeneous lattice expansion over the **b** axis (sample thickness) in the 10 ns−10 µs time window. At 50 µs the temperature is homogenized over the crystal and the heating effect results in thermal population of the HS state.

Table 1

Geometry changes for the monoclinic polymorph on excitation based on the LASER refinement of the 50 μs data. The accuracy of the excited state molecular distances was estimated by error propagation.

Contact	*Bond length* / Å	
	GS	ES
Fe1-O1	1.866(2)	1.92(2)
Fe1-O2	1.915(2)	1.83(3)
Fe1-N1	1.977(3)	2.03(6)
Fe1-N2	2.031(3)	2.13(3)
Fe1-N3	1.982(3)	2.02(3)
Fe1-N4	1.989(3)	2.04(3)
	Shift / Å	
Fe1-Fe1E	0.17(2)	
N1-N1E	0.11(5)	
N2-N2E	0.05(5)	
N3-N3E	0.07(3)	
N4-N4E	0.08(4)	
O1-O1E	0.14(2)	
O2-O2E	0.12(2)	